Edinburgh Research Explorer

Orientation Model of Mobile Device for Indoor VLC and Millimetre Wave Systems

Orientation Model of Mobile Device for Indoor VLC and Millimetre Wave Systems

Zhihong Zeng, Mohammad Dehghani Soltani, Harald Haas and Majid Safari

School of Engineering, Institute for Digital Communications, LiFi R&D Centre, The University of Edinburgh

E-mail: {zhihong.zeng, m.dehghani, h.haas, majid.safari}@ed.ac.uk

Abstract—**Visible light communications (VLC) and Millimetre wave (mmWave) systems are two emerging technologies for short-range mobile communications. One of the limiting factors of both VLC and mmWave systems is the random orientation of mobile devices that can significantly affect the channel gain in both systems. Since there is no proper model for device orientation, many studies have assumed that device orientation is fixed or modelled as a uniform distribution. To address this issue, an experimental study of mobile user behaviour is conducted and a statistical orientation model is proposed in this paper. The results show that the probability density function (PDF) of the elevation angle follows a Laplace distribution. Based on the statistical orientation model, Monte-Carlo simulations are carried out to analyse the system performance of VLC and mmWave systems. The statistics of signal-to-noise-ratio (SNR) are compared with the experiment-based simulation results in both VLC and mmWave systems.**

Index Terms—**LiFi, Laplace distribution, millimetre wave communication, optical wireless communication.**

I. INTRODUCTION

To support the ever-growing wireless demand, which is anticipated to be 49 exabytes by 2021 [1], techniques such as Millimetre wave communications (mmWave) and Light-Fidelity (LiFi) are being explored. LiFi is a promising novel bidirectional, high-speed and fully networked wireless communication technology [2], [3]. Large and unregulated bandwidth are available in the visible light spectrum. High energy efficiency and the simple deployment of LiFi with off-the-shelf light emitting diodes (LEDs), enhanced security as the light can not penetrate through opaque objects, are some advantages of LiFi compared to radio frequency (RF) systems [4]. Millimetre wave is another promising technology with the frequency range between 30 and 300 GHz to support the future next-generation high-speed wireless communications. Some notable advantages of mmWave include: the availability of RF bandwidth and the very small wavelengths that permit embedding large numbers (typically 32 elements) of miniaturized antennas within small spaces. This leads to reduced hardware size for antenna beamforming systems needed [5].

Statistical data traffic confirms that smartphones are the most significant source for generated mobile traffic. It is envisaged that smartphones will generate more than 42 exabytes per month (86% of the mobile data traffic) [1]. LiFi and mmWave as part of future fifth generation (5G) of mobile networks can cope with this immense data traffic thanks to future LiFi-enabled and mmWave-enabled smart phones. One of the key challenges facing both LiFi and mmWave is the lack

of a convenient statistical model for device orientation. Users usually prefer to work with their smartphones in a comfortable manner with any orientation which means that the device is not necessarily always pointed vertically upward.

Many previous studies on LiFi and mmWave systems consider simplified assumptions due to the lack of a proper model for device orientation. In LiFi systems, it is commonly assumed that the receiver is directed towards the access point (AP) and is fixed. However, there are a few studies that have emphasised the effect of device orientation in their analysis [6]–[10]. All these studies consider the elevation angle as a random variable without discussing the actual statistics of it, such as its mean and variance. In mmWave networks, many studies assume that the angle of arrival (AoA) follows a uniform distribution [11], [12]. The authors in [13] proposed a new algorithm to obtain the three dimensional (azimuth and elevation) angles of arrival (AoA) for dynamic indoor terahertz (THz) channels. The indoor THz channel dynamic depends on human movement and the statistics of human motion have been obtained based on data measurements. However, their model is specified based on three particular scenarios and no general model for the elevation angle has been proposed.

Contributions: In this paper, a novel model for the mobile device orientation based on the experimental measurement is proposed. The model can be used for both visible light communications (VLC) and mmWave networks. The accuracy of the model is tested by using the Kolmogorov-Smirnov distance (KSD) and skewness tests. We also provide some results that show the significant effect of considering the random orientation of a mobile device on network parameters such as signal-to-noise-ratio (SNR) in a single AP or base station (BS) VLC and mmWave systems.

II. SYSTEM MODEL

Both VLC and mmWave systems are considered in this study. For simplification, the single AP/BS system is used. Network level analysis will be considered in future studies. The downlink geometry of the line of sight (LOS) link is shown in Fig. 1. The position vector, $\mathbf{p}_\mathrm{a} = (x_\mathrm{a}, y_\mathrm{a}, z_\mathrm{a})$, is the location of the AP/BS, and $\mathbf{p}_\mathrm{m} = (x_\mathrm{m}, y_\mathrm{m}, z_\mathrm{m})$ is the position vector of the mobile device (MD). The angle, ϕ, is the radiance angle of the transmitter, also known as the angle of departure (AoD). The angle, ψ, is the incidence angle of the receiver, or can be known as the angle of arrival (AoA). The distance vector between the user equipment and the AP is defined as
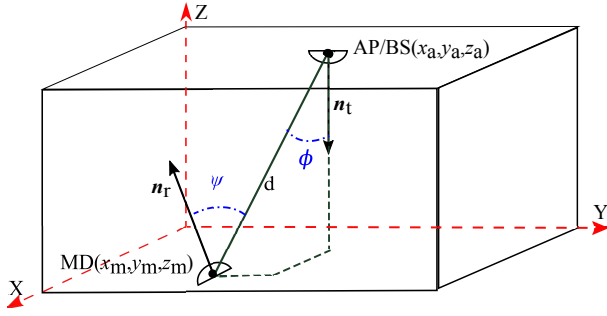
Fig. 1: Downlink geometry of LOS light propagation.

$\mathbf{d} = \mathbf{p}_a - \mathbf{p}_m$. The unit normal vectors of the transmitter and receiver surface are denoted as $\mathbf{n}_t$ and $\mathbf{n}_r$ respectively. The dot product is denoted as $(\cdot)$. Denoting the Euclidean distance by $\|\mathbf{d}\|$, the ψ and ϕ angles are separately given by:

$$\cos(\psi) = \frac{\mathbf{n}_r \cdot \mathbf{d}}{\|\mathbf{d}\|}, \qquad (1)$$

$$\cos(\phi) = -\frac{\mathbf{n}_t \cdot \mathbf{d}}{\|\mathbf{d}\|}. \qquad (2)$$

A. VLC system model

In most VLC systems, the signal is dominated by the component received from the LOS path (if not blocked) when the receiver is not as close to the walls. The direct-current (DC) channel gain can be used to model the VLC system channel. It is assumed that the LED follows the Lambertian radiation. The LOS DC gain is given by [14]:

$$H_{\text{VLC}} = \begin{cases} \frac{(m+1)A}{2\pi d^2} \cos^m(\phi) \cos(\psi) & \text{if } 0 \leq \psi \leq \Psi_c \\ 0 & \text{if } \psi > \Psi_c \end{cases}, \quad (3)$$

where A is the physical area of the photodiode (PD); the Lambertian order, m, is given as $m = -\ln(2)/\ln(\cos(\Phi_{1/2}))$; $\Phi_{1/2}$ denotes the half-power semi-angle of the LED; the field of view (FOV) of the PD is denoted as Ψ_c. The noise is assumed to follow a white Gaussian distribution with the power spectral density of N_0. The SNR at the receiver of LiFi systems can be calculated as [15]:

$$\xi_{\text{VLC}} = \frac{(RH_{\text{VLC}}P_{\text{t,optical}})^2}{\sigma_{\text{VLC}}^2}, \qquad (4)$$

where $P_{\text{t,optical}}$ is the transmitted optical power of the AP and R represents the PD responsivity. The total noise power is given as $\sigma_{\text{VLC}}^2 = N_0 B_{\text{VLC}}$, where B_{VLC} is the utilized VLC bandwidth [14].

B. Millimetre wave system model

In general, an indoor mmWave link can be described using a geometric channel model with L scatterers as introduced in [16], [17]. It is assumed that each scatterer contributes a single propagation path and the directional beamforming technique is used [18]. Here, we assume a simplified scenario by considering a single path mmWave channel (i.e., $L = 1$). The virtual channel model can be transformed from the geometrical channel model and it is given as follows [11]:

$$\mathbf{H}_{\text{mmWave}} = \alpha \sqrt{N_{\text{BS}} N_{\text{MD}}} \mathbf{a}_{\text{MD}}(\psi) \mathbf{a}_{\text{BS}}^*(\phi), \qquad (5)$$

where the complex value α denotes the channel attenuation, which includes the path-loss. Note that $|\alpha|^2 = (\frac{d}{d_0})^2 |\alpha_0|^2$, where $|\alpha|^2 = 10^{-7}$ at $d_0 = 1$ m [12]. N_{BS} and N_{MD} represent the number of antenna in the single base station and the mobile device respectively. In addition, $\mathbf{a}_{\text{MD}}(\psi)$ and $\mathbf{a}_{\text{BS}}(\phi)$ are the antenna array response vectors of MD and BS respectively. It is assumed that the uniform linear array is used, and * denotes the Hermitian of matrix. $\mathbf{a}_{\text{MD}}(\psi)$ and $\mathbf{a}_{\text{BS}}(\phi)$ can be defined as [11]:

$$\mathbf{a}_{\text{MD}}(\psi) = \frac{[1, e^{j\frac{2\pi}{\lambda}d_{\text{ant}}\sin\psi}, ..., e^{j(N_{\text{MD}}-1)\frac{2\pi}{\lambda}d_{\text{ant}}\sin\psi}]^{\text{T}}}{\sqrt{N_{\text{MD}}}}, \quad (6)$$

$$\mathbf{a}_{\text{BS}}(\phi) = \frac{[1, e^{j\frac{2\pi}{\lambda}d_{\text{ant}}\sin\phi}, ..., e^{j(N_{\text{BS}}-1)\frac{2\pi}{\lambda}d_{\text{ant}}\sin\phi}]^{\text{T}}}{\sqrt{N_{\text{BS}}}}, \quad (7)$$

where λ represents the wavelength of the signal; d_{ant} denotes the distance between adjacent antennas and $[\cdot]^{\text{T}}$ denotes the transpose operation. Then, the SNR in mmWave systems can be obtained as follows [11]:

$$\xi_{\text{mmWave}} = \frac{P_{\text{t,mmWave}} |\boldsymbol{w}_u^* \mathbf{H}_{\text{mmWave}} \mathbf{B}|^2}{\sigma_{\text{mmWave}}^2}, \qquad (8)$$

where $P_{\text{t,mmWave}}$ is the BS transmit power, $\boldsymbol{w}_u$ is the RF combining vector and $\mathbf{B}$ is the precoder matrix. σ_{mmWave}^2 is the noise power. In this study, we consider a mmWave system consisting of two antennas in both BS and MD. The separation distance, d_{ant}, is assumed to be half of the signal wavelength. In addition, assuming that the BS can perfectly point the beam towards the user (i.e., $\mathbf{B} = \frac{1}{2}[1, e^{j\pi\sin\phi}]^{\text{T}}$) while the user can only estimate the average orientation of the mobile device (i.e., $\boldsymbol{w}_u = \frac{1}{2}[1, e^{j\pi\mathbb{E}_\psi[\sin\psi]}]^{\text{T}}$), (8) can be simplified as:

$$\xi_{\text{mmWave}} = \frac{|\alpha|^2 P_{\text{t,mmWave}} |1 + e^{j\pi(\sin\psi - \mathbb{E}_\psi[\sin\psi])}|^2}{4\sigma_{\text{mmWave}}^2}. \quad (9)$$

C. Role of device orientation

As it is apparent from Fig. 1, the normal vector $\mathbf{n}_r$ changes with the device orientation and accordingly the angle ψ changes as well. As shown in (3) and (5), the channel gain of both systems are related to the angle ψ. Hence, the orientation of a device will affect the received SNR and thus affect the performance of both systems. In effect, the orientation of mobile devices plays an important role in both indoor VLC systems and mmWave systems, which provides the motivation behind this study.

III. ROTATION GEOMETRY

According to Euler's rotation theorem, the rotation of a 3D body can be described by three elemental angles: yaw, pitch, and roll. The extrinsic rotation is the rotation about the Earth coordinate system, XYZ, while the intrinsic rotation corresponds to the rotation about the device corrdinate system, xyz. Fig. 2(a) and Fig. 2(b) illustrate the Earth and device co-ordinate system respectively. When viewed along the positive direction of an axis, the positive rotation means that the object rotates clockwise around this axis. As shown in Fig. 2(b)-(d), yaw is the positive rotation around the z-axis with an angle of
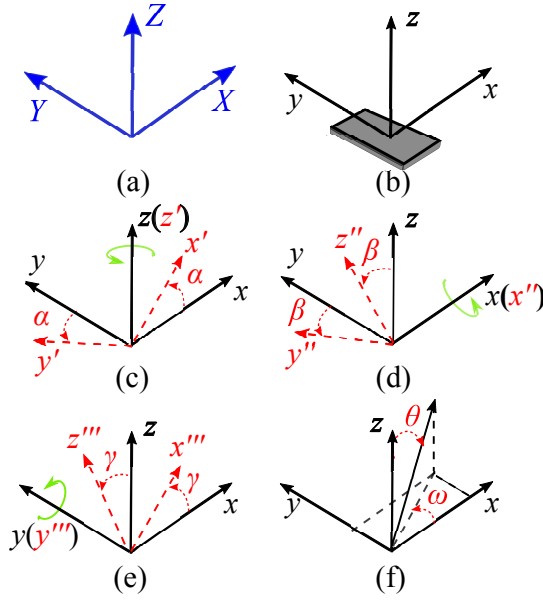
Fig. 2: Coordinate system and orientation of a mobile device: (a) the Earth coordinate system, (b) the device coordinate system, (c) yaw, α, (d) pitch, β, (e) roll, γ (f) the spherical coordinate system.

α; pitch is the positive rotation around the x-axis with an angle of β; roll is the positive rotation around the y-axis with an angle of γ. The range of α, β, γ are $[0°, 360°)$, $[-180°.180°)$, $[-90°, 90°]$ respectively. Yaw, pitch and roll can be described by matrices and are denoted as $\mathbf{R}(\alpha)$, $\mathbf{R}(\beta)$, $\mathbf{R}(\gamma)$ separately as [19]:

$$\mathbf{R}(\alpha) = \begin{bmatrix} \cos\alpha & -\sin\alpha & 0 \\ \sin\alpha & \cos\alpha & 0 \\ 0 & 0 & 1 \end{bmatrix}, \qquad (10)$$

$$\mathbf{R}(\beta) = \begin{bmatrix} 1 & 0 & 0 \\ 0 & \cos\beta & -\sin\beta \\ 0 & \sin\beta & \cos\beta \end{bmatrix}, \qquad (11)$$

$$\mathbf{R}(\gamma) = \begin{bmatrix} \cos\gamma & 0 & \sin\gamma \\ 0 & 1 & 0 \\ -\sin\gamma & 0 & \cos\gamma \end{bmatrix}. \qquad (12)$$

According to the world wide web consortium (W3C) specification, the intrinsic rotation of the device should follow the order of yaw, pitch and then roll, so by multiplying $\mathbf{R}(\alpha)$, $\mathbf{R}(\beta)$, $\mathbf{R}(\gamma)$ in sequence, the whole rotation can be denoted as: $\mathbf{R}(\alpha, \beta, \gamma) = \mathbf{R}(\alpha)\mathbf{R}(\beta)\mathbf{R}(\gamma)$. The initial unit normal vector of the PD on a device, $\mathbf{n}_z$, is $[0, 0, 1]^T$. After the rotation of the device, the unit normal vector is given by:

$$\mathbf{n}_r = \mathbf{R}(\alpha, \beta, \gamma)\mathbf{n}_z = \begin{bmatrix} \cos\gamma \sin\alpha \sin\beta + \cos\alpha \sin\gamma \\ \sin\alpha \sin\gamma - \cos\alpha \cos\gamma \sin\beta \\ \cos\beta \cos\gamma \end{bmatrix} \quad (13)$$

In the spherical coordinate system, as shown in Fig. 2(f) the unit normal vector $\mathbf{n}_r$ can be represented by an azimuth angle, ω, and an elevation angle, θ. The elevation angle is the angle between the unit normal vector of the mobile device and the unit vector of the Z axis, $[0, 0, 1]^T$. Based on (13), the elevation angle is thus given by:

$$\theta = \arccos(\cos\beta \cos\gamma), \qquad (14)$$

Equation (14) shows that the elevation angle only depends on the pitch angle, β, and the roll angle, γ. A change in the yaw angle has no effect on the elevation angle, θ. The range of ω and θ is 0° to 360° and 0° to 90°, respectively. Alternatively, the unit normal vector $\mathbf{n}_r$ can be expressed as:

$$\mathbf{n}_r = [\sin\theta \cos\omega, \sin\theta \sin\omega, \cos\theta]^T \qquad (15)$$

Substituting (15) into (1), the ψ angle can be described in terms of the elevation and azimuth angles. The azimuth angle indicates the direction that the user faces and therefore it is reasonable to assume that ω is uniformly distributed in [0, 360°]. This has been also confirmed with our measurement results [20]. In the following sections, we will provide a model for the elevation angle based on the experimental measurements.

IV. ORIENTATION DATA COLLECTION

Since we are interested in the random orientation of mobile devices, the data collection process should not interfere with users' behaviour. There are three fundamental requirements for the mobile phone application: i) the application should record the orientation data using built-in sensors; ii) in relation to the recording speed, the amount of data collected in one second should be sufficient, as the changing speed of orientation will also affect the final channel model; iii) the application is required to record the orientation data under background conditions so that participants can use their phones as usual during the data collection process. The mobile phone application, Physics Toolbox Sensor Suite, developed by Vieyra Software [21] has been used to collect the instantaneous orientation angles of roll, pitch and yaw. Another important characteristic of this application is its ability to run in the background without interrupting users' normal activities.

Simple random sampling is the fundamental method of probability sampling. In the random sampling theory, the chance of being chosen as a sample is independent and equal for every element in the population of interest [22]. In the experiment test, 20 volunteers were recruited randomly to participate in the data collection. As the purpose of this experiment is to develop a channel model for wireless communication systems, the only rule was that users had to sit in an indoor environment and use their mobile phones for daily activities, e.g. chatting, browsing, gaming, or watching videos. To ensure nothing influenced the data collection process, there was no extra control placed on the experimental place, time, or activities. The whole process is random, so the participants have complete freedom to use their cellphones as they normally would. Random sampling makes the data collected more reliable. The total number of samples recorded for each angle is around 600,000. To build up a model for users device orientation, data should be collected when participants use their phone for daily activities. However, during the data collecting process, some redundant data will be recorded. After removing the redundant data, there are around 570,000 samples for each angle. The following studies are carried out based on these reliable samples.
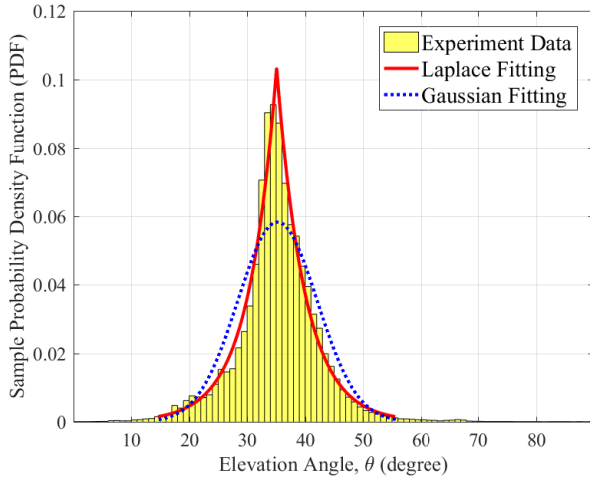
Fig. 3: Sample PDF of elevation angle, Laplace distribution fit and Gaussian distribution fit.

TABLE I: Parameters of different fits

	Laplacian Fitting	Gaussian Fitting
μ	35.09°	35.23°
σ	7.01°	7.65°
KSD	0.03	0.08
Skewness	0.29	
Kurtosis	6.46	

TABLE II: Parameters Lists

Parameter	Symbol	Value
Transmitted optical power per AP	$P_{\text{t,optical}}$	1 W
Modulated bandwidth for LED	B_{VLC}	20 MHz
Physical are of the PD	A	1 cm^2
Receiver FOV semi-angle	Ψ_c	90°
Half-intensity radiation angle	$\Phi_{1/2}$	60°
PD responsivity	R	0.5 A/W
Noise spectral density for VLC	N_0	10^{-21} A^2/Hz
mmWave BS transmit power	$P_{\text{t,mmWave}}$	30 dBm
mmWave carrier frequency	v	73 GHz
mmWave bandwidth	B_{mmWave}	2 GHz
Noise power for mmWave	σ_{mmWave}^2	-174 dBm/Hz + $10\log_{10}(B_{\text{mmWave}})$ + noise figure of 10 dB

V. STATISTICAL MODEL

It is shown in [23] that the Laplace distribution, as the first law of error, and the Gaussian distribution, as the second law of error, are two good approximation models for the magnitude of error. Thus, both Laplace and Gaussian distribution are used to model the probability density function (PDF) of the elevation angle [23]. Parameters of the Laplacian and Gaussian fittings are defined and calculated according to the maximum likelihood estimation [24]. To determine the goodness-of-fit of a reference probability distribution, the Kolmogorov-Smirnov (K-S) test is used as it is one of the most useful non-parametric tests [25]. The K-S test gives a Kolmogorov-Smirnov distance (KSD) which represents the difference between the reference cumulative distribution function and the empirical cumulative distribution function. Skewness describes the level of symmetry for the values spread around the mean. Kurtosis describes the peakedness of the empirical probability distribution [26].

Based on the collected pitch and roll samples, we can calculate the elevation angle, θ according to (14). The histogram of θ is plotted in Fig. 3. Both Laplace and Gaussian fits are shown in the figure. KSD is calculated by comparing the difference between the empirical cumulative distribution functions of two sets of samples. The first are the experimentally measured samples, and the other are samples generated from the reference distribution. The results are summarised in Table I. As expected, the histogram of the elevation angle is almost symmetric, as the skewness has a small value. With regards to kurtosis, Laplace distribution is a better model as 6.46 indicates a higher peak than a normal distribution with a kurtosis of 3. It can be seen that the Laplace distribution has a better goodness-of-fit in terms of KSD. Based on the above analysis, the PDF of the elevation angle is modelled with a Laplace distribution. From the parameters in Table I, $\mu = 35.09°$, $b = \sqrt{\frac{\sigma^2}{2}} = 4.82°$. The statistical model for the elevation angle is thus denoted as:

$$f(\theta) = \frac{\exp\left(-\frac{|\theta-\mu|}{b}\right)}{2b}, \quad 0 \leq \theta \leq \frac{\pi}{2} \tag{16}$$

It is noted that the main conclusions of the paper are confirmed by our controlled experimental tests reported in [20].

VI. SIMULATION RESULTS

In this section, based on the statistical model, the performance of both VLC and mmWave systems with single AP/BS are analysed, and the results are compared with orientation models used in other studies.

A. VLC System with single AP

The performance of a VLC system with the constant vertical orientation model, the experimental orientation model and the statistical orientation model are compared to see how device orientation can influence the system performance. The simulation environment is assumed to be a room of size 5 m × 5 m × 3 m. The location of the LED is $(2.5, 2.5, 3)$. The height of the mobile device is assumed to be 0.8 m from the floor. The testing points are evenly chosen with a spacing of 0.1 m between them. Based on the typical settings and parameters in Table II, Monte-Carlo simulations are carried out to analyse the system performance numerically.

In the constant vertical orientation model, the device at each testing point is perpendicular to the ceiling, and the normal vector of PD is $[0, 0, 1]^{\text{T}}$. SNR can be calculated based on (3) and (4). For each orientation model, the average SNR is calculated for each testing point. The cumulative distribution function (CDF) of the average SNR is plotted in Fig. 4. The CDF of the statistical model and the experimental model are almost overlapping with each other, with a maximum difference of 0.045 dB. Thus, the statistical model proposed achieves higher accuracy and is a good estimation of the random orientation model. In contrast, the maximum difference
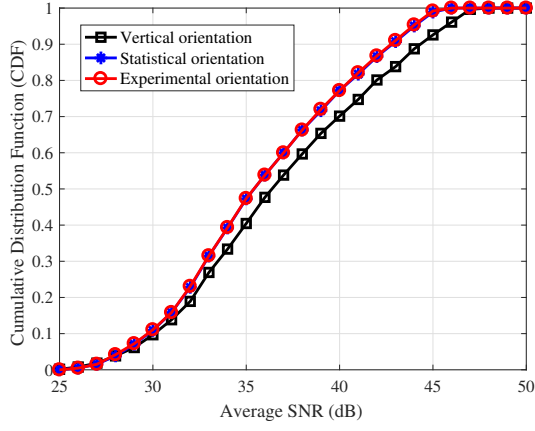
Fig. 4: CDF of the average SNR for the vertical orientation model, the statistical orientation model and the experimental orientation model.
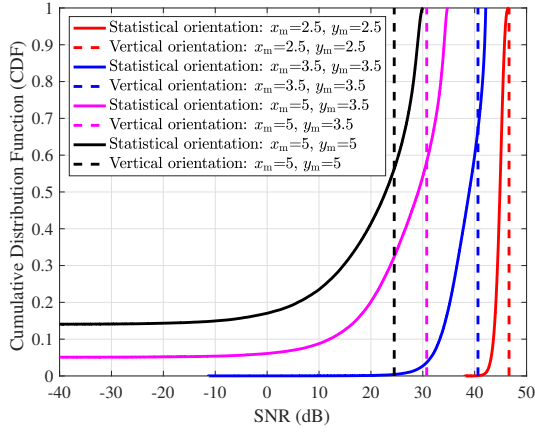

Fig. 5: CDF of the SNR for different locations.

between the experimental model and the vertical model is 2 dB suggesting that the traditional vertical orientation model is a poor estimation of the random orientation. The effect of orientation for different locations is observed and the results are plotted in Fig. 5. In the vertical orientation model, the SNR is fixed for each location, so the CDF will be a vertical line. As the horizontal distance between the AP and the user increases, the CDFs of the SNR for the statistical model will deviate further away from the CDFs of the SNR for the vertical orientation. Hence, orientation plays a more important role when the users are far away from the APs. Fig. 6 compares the SNR between the experiment-based simulation and the statistic-based simulation for 4 user positions with a fixed $\omega = \frac{5\pi}{4}$ as an example. The simulation results of PDF of SNR based on the experimental orientation and the statistical model are matched.

B. mmWave System with single base station

In this section, SNR of the mmWave system is compared and analysed for different orientation models. The simulation environment is the same as in the single AP VLC system. The parameters are shown in Table II. The Monte-Carlo simulation results of three orientation models are compared
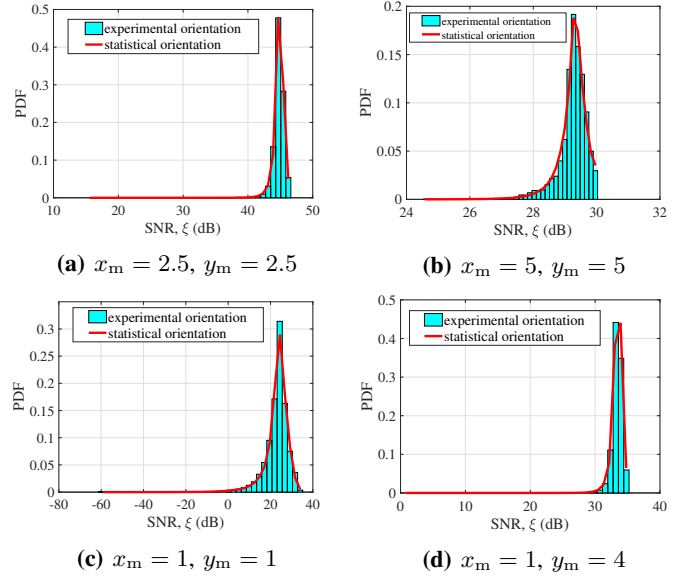

(a) $x_{\mathrm{m}} = 2.5$, $y_{\mathrm{m}} = 2.5$ **(b)** $x_{\mathrm{m}} = 5$, $y_{\mathrm{m}} = 5$

(c) $x_{\mathrm{m}} = 1$, $y_{\mathrm{m}} = 1$ **(d)** $x_{\mathrm{m}} = 1$, $y_{\mathrm{m}} = 4$

Fig. 6: Comparison between simulation results of PDF of SNR, ξ, for 4 user positions with $\omega = \frac{5\pi}{4}$ based on the experimental orientation and the statistical orientation model.
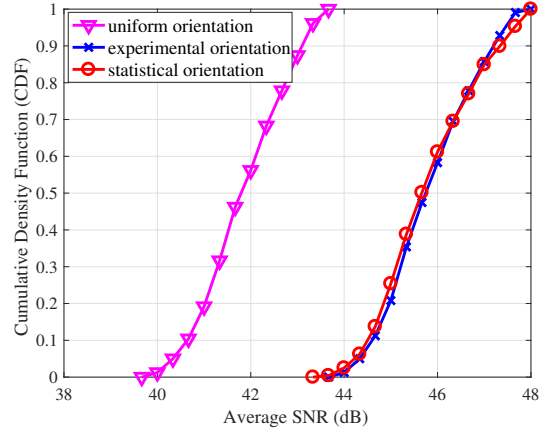

Fig. 7: CDF of the average SNR for the uniform orientation model, the statistical orientation model and the experimental orientation model.

in this section: the uniform model, experimental data and the proposed Laplace model. The uniform orientation model is used in [11], where AoA, ψ, is assumed to be uniformly distributed in $\left[-\frac{\pi}{2}, \frac{\pi}{2}\right]$, and the azimuth angle, ω is uniformly distributed in $[0, 2\pi]$. For each orientation model, the average SNR is calculated for each testing point. The CDF of the average channel gain is plotted in Fig. 7. The simulation results of the proposed statistical model represent the results of the measured random orientation much better than the uniform orientation model. Fig. 8 compares the SNR between the experiment-based simulation results and the statistic-based simulation results according to (9). The results are given for 4 user positions with a fixed $\omega = \frac{\pi}{4}$ as an instance. The simulation results of PDF of SNR based on the experimental orientation and the statistical model are matched.
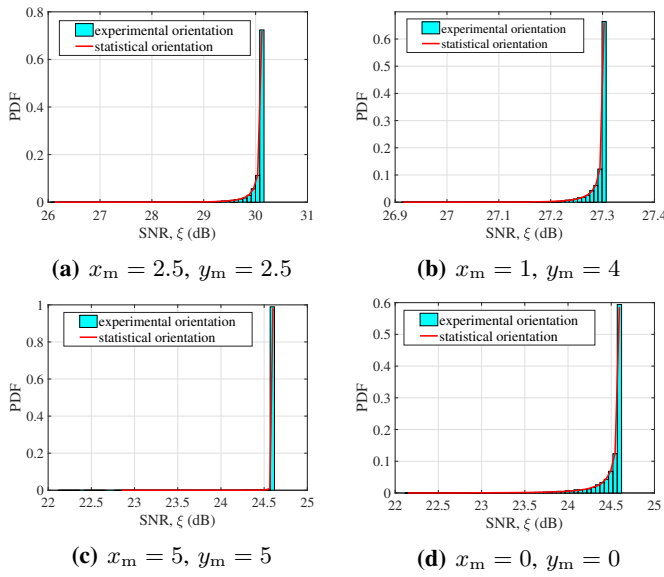
(a) $x_\mathrm{m} = 2.5$, $y_\mathrm{m} = 2.5$

(b) $x_\mathrm{m} = 1$, $y_\mathrm{m} = 4$

(c) $x_\mathrm{m} = 5$, $y_\mathrm{m} = 5$

(d) $x_\mathrm{m} = 0$, $y_\mathrm{m} = 0$

Fig. 8: Comparison between simulation results of PDF of SNR for 4 user positions with $\omega = \frac{\pi}{4}$ based on the experimental orientation and the statistical orientation model.

VII. CONCLUSION

The importance of device orientation in relation to the system performance of VLC and mmWave systems is shown. It is noted that there is a significant gap between the SNR performance of a system considering the random orientation and the traditional model in which the device is assumed to be fixed or modelled as uniformly distributed. Based on the measurements, a Laplace model for the elevation angle of mobile devices is proposed and it is seen that the Laplace model fits the measurements very well. The model can be used in both VLC and mmWave systems to obtain the statistics of these systems such as channel gain and SNR. The system performance (i.e., signal to interference noise ratio, achievable data rate and handover probability) of LiFi networks and mmWave networks based on the proposed orientation model will be studied in future works.

VIII. ACKNOWLEDGMENT

REFERENCES

[1] Cisco, "Cisco Visual Networking Index: Global Mobile Data Traffic Forecast Update, 2016–2021 White Paper," *white paper at Cisco.com*, Mar. 2017.

[2] H. Haas, L. Yin, Y. Wang, and C. Chen, "What Is LiFi?" *Journal of Lightwave Technology*, vol. 34, no. 6, pp. 1533–1544, March 2016.

[3] M. D. Soltani, X. Xu, M. Safari, and H. Haas, "Bidirectional User Throughput Maximization Based on Feedback Reduction in LiFi Networks," *IEEE Transactions on Communications*, pp. 1–1, 2018.

[4] S. Wu, H. Wang, and C. H. Youn, "Visible Light Communications for 5G Wireless Networking Systems: From Fixed to Mobile Communications," *IEEE Network*, vol. 28, no. 6, pp. 41–45, Nov 2014.

[5] Z. Pi and F. Khan, "An Introduction to Millimeter-wave Mobile Broadband Systems," *IEEE Communications Magazine*, vol. 49, no. 6, pp. 101–107, June 2011.

[6] M. D. Soltani, X. Wu, M. Safari, and H. Haas, "Access Point Selection in Li-Fi Cellular Networks with Arbitrary Receiver Orientation," in *2016 IEEE 27th Annual International Symposium on Personal, Indoor, and Mobile Radio Communications (PIMRC)*, Valencia, Spain, Sept 2016, pp. 1–6.

[7] M. D. Soltani, H. Kazemi, M. Safari, and H. Haas, "Handover Modeling for Indoor Li-Fi Cellular Networks: The Effects of Receiver Mobility and Rotation," in *2017 IEEE Wireless Communications and Networking Conference (WCNC)*, San Fransisco, USA, March 2017, pp. 1–6.

[8] J. Y. Wang, Q. L. Li, J. X. Zhu, and Y. Wang, "Impact of Receiver's Tilted Angle on Channel Capacity in VLCs," *Electronics Letters*, vol. 53, no. 6, pp. 421–423, Mar. 2017.

[9] J. Y. Wang *et al.*, "Improvement of BER Performance by Tilting Receiver Plane for Indoor Visible Light Communications with Input-Dependent Noise," in *2017 IEEE International Conference on Communications (ICC)*, Paris, France, May 2017, pp. 1–6.

[10] E.-M. Jeong *et al.*, "Tilted Receiver Angle Error Compensated Indoor Positioning System Based on Visible Light Communication," *Electronics Letters*, vol. 49, no. 14, pp. 890–892, 2013.

[11] A. Alkhateeb, G. Leus, and R. W. Heath, "Limited Feedback Hybrid Precoding for Multi- User Millimeter Wave Systems," *Wireless Communications, IEEE Transactions on*, vol. 14, no. 11, pp. 6481–6494, 2015.

[12] S. Singh, M. N. Kulkarni, A. Ghosh, and J. G. Andrews, "Tractable Model for Rate in Self- Backhauled Millimeter Wave Cellular Networks," *Selected Areas in Communications, IEEE Journal on*, vol. 33, no. 10, pp. 2196–2211, 2015.

[13] B. Peng and T. Krner, "Three-Dimensional Angle of Arrival Estimation in Dynamic Indoor Terahertz Channels Using a Forward-Backward Algorithm," *IEEE Transactions on Vehicular Technology*, vol. 66, no. 5, pp. 3798–3811, May 2017.

[14] J. M. Kahn and J. R. Barry, "Wireless Infrared Communications," *Proceedings of the IEEE*, vol. 85, no. 2, pp. 265–298, 1997.

[15] T. Komine and M. Nakagawa, "Fundamental Analysis for Visible- Light Communication System Using LED Lights," *Consumer Electronics, IEEE Transactions on*, vol. 50, no. 1, pp. 100–107, 2004.

[16] T. S. Rappaport, R. Shu Sun, Y. Mayzus, K. Hang Zhao, G. N. Azar, J. K. Wang, M. Wong, F. Schulz, F. Samimi, and F. Gutierrez, "Millimeter Wave Mobile Communications for 5G Cellular: It Will Work!" *Access, IEEE*, vol. 1, pp. 335–349, 2013.

[17] T. S. Rappaport *et al.*, "Broadband Millimeter-Wave Propagation Measurements and Models Using Adaptive-Beam Antennas for Outdoor Urban Cellular Communications," *IEEE Transactions on Antennas and Propagation*, vol. 61, no. 4, pp. 1850–1859, April 2013.

[18] O. E. Ayach, S. Rajagopal, S. Abu-Surra, Z. Pi, and R. W. Heath, "Spatially Sparse Precoding in Millimeter Wave MIMO Systems," *IEEE Transactions on Wireless Communications*, vol. 13, no. 3, pp. 1499–1513, March 2014.

[19] S. M. LaValle, *Planning Algorithms*. Cambridge: Cambridge : Cambridge University Press, 2006.

[20] M. D. Soltani, A. A. Purwita, Z. Zeng, H. Haas, and M. Safari, "Modeling the Random Orientation of Mobile Devices: Measurement, Analysis and LiFi Use Case," *submitted to IEEE Transactions on Communications*.

[21] Physics Toolbox Sensor Suite. Vieyra Software. [Online]. Available: https://play.google.com/store/apps/details?id=com.chrystianvieyra.physicstoolboxsuite

[22] R. Sapsford and V. Jupp, *Data Collection and Analysis*. Sage, 2006.

[23] S. Kotz, T. Kozubowski, and K. Podgorski, *The Laplace Distribution and Generalizations: A Revisit with Applications to Communications, Economics, Engineering, and Finance*. Springer Science & Business Media, 2012.

[24] C. Chen, "TESTS FOR THE GOODNESS-OF- FIT OF THE LAPLACE DISTRIBUTION," *Communications in Statistics - Simulation and Computation*, vol. 31, no. 1, pp. 159–174, 2002.

[25] D. L. Evans, J. H. Drew, and L. M. Leemis, *The Distribution of the Kolmogorov–Smirnov, Cramer–von Mises, and Anderson–Darling Test Statistics for Exponential Populations with Estimated Parameters*. Cham: Springer International Publishing, 2017, pp. 165–190.

[26] H.-M. Kaltenbach, *Basics of Probability Theory*. Berlin, Heidelberg: Springer Berlin Heidelberg, 2012, pp. 1–27.